Illinois State University
ISU ReD: Research and eData

Faculty publications – Physics

Physics

5-15-2001

Phonon modes in InAs quantum dots

Shang-Fen Ren
Illinois State University

G Qin
Illinois State University

Deyu Lu
University of Illinois at Urbana-Champaign

Follow this and additional works at: http://ir.library.illinoisstate.edu/fpphys

Part of the Condensed Matter Physics Commons

Phonon modes in InAs quantum dots

Shang-Fen Ren

Department of Physics, Illinois State University, Normal, Illinois 61790-4560

Deyu Lu

Department of Physics, University of Illinois at Urbana-Champaign, 1110 W. Green Street, Urbana, Illinois 61801

G. Qin

Department of Physics, Illinois State University, Normal, Illinois 61790-4560
Department of Physics, Nanjing University, Nanjing, People's Republic of China

Phonon modes in spherical InAs quantum dots (QDs) with up to 11 855 atoms (about 8.5 nm in diameter) are calculated by using a valence force field model, and all the vibration frequencies and vibration amplitudes of the QDs are calculated directly from the lattice-dynamic matrix. The projection operators of the irreducible representations of the group theory are employed to reduce the computational intensity, which further allows us to investigate the quantum confinement effect of phonon modes with different symmetries. It is found that the size effects of phonon modes depend on the symmetry of the modes. For zinc-blende structure, the modes with A_1 symmetry has the strongest quantum confinement effect and the T_1 mode the weakest. There could be a crossover of symmetries of the highest frequencies from A_1 to T_2 as the size of the QDs decreases. The behavior of vibration amplitudes and vibration energies of phonon modes in different symmetries are also investigated in detail. These results provide microscopic details of the phonon properties of QDs that are important to the fundamental understanding and potential applications of semiconductor QDs.

I. INTRODUCTION

Low-dimensional semiconductor structures have attracted much research attention in recent years because of their importance in the fundamental understanding of physics and potential applications. Semiconductor quantum dots (QDs) have many potential applications in electronic devices, information processing, and nonlinear optics. The electronic properties of QDs have been intensively studied in recent years, both theoretically and experimentally, and a clear understanding of much of the basic physics of the quantum confinement effects of electrons in QDs has been achieved.[1] On the other hand, the vibration properties of QDs, i.e., the confinement of phonon modes in QDs, are less understood.

On the experimental side, several spectroscopic techniques, including Raman scattering, power-dependent photoluminescence (PL) and photoluminescence excitation (PLE) have been used to investigate confined longitudinal-optical (LO) phonons, surface optical phonons, and confined acoustic-phonon modes.[2–16] There is considerable experimental evidence for the confinement effects of phonon modes in low-dimensional systems. For example, the lattice softening of the LO phonon modes was observed by resonant Raman spectroscopy.[12,13] On the other hand, the PL and PLE spectra of self-organized InAs/GaAs QDs indicate an apparent increase of LO phonon frequencies as the dots get smaller, attributed to the large strain in the small dots. There are also experimental observations that the phonon modes in the low-frequency range in small QDs depends on the size of QDs,[6,14] and the phonon frequencies are dependent on both the host matrix and the size of the QDs.[16]

On the theoretical side, a few studies of phonon modes in QDs have appeared. Most theoretical models so far treat optical phonons with the macroscopic continuum model and some *ad hoc* boundary conditions. Thus, the analytic expression of the eigenfunctions of LO phonons and surface optical phonons of small spherical,[10,17–23] and cylindrical[24] QDs are derived and the electron-phonon interactions are calculated. But these models deal with only optical phonons, not acoustic phonons. Strictly speaking, the distinction between optical and acoustic phonon modes is only meaningful in the long-wavelength limit. For QDs of nanometer sizes, we really have to consider all the realistic phonon modes as a whole to understand the vibration properties. Recently, a microscopic treatment of phonon modes in GaP QDs was described, which provides a theoretical explanation to several experimental observations.[25] However, because of the computational intensity, only phonon modes in QDs with up to 2000 atoms are studied. In some way, our theoretical treatment of phonon modes in QDs is similar to this treatment. One important difference is that we employed the projection operators of the irreducible representations of the group theory to reduce the computational intensity. Not only does this allow us to investigate phonon modes in QDs with a much larger size, but it also helps us to reveal some important physics that otherwise could not be revealed.

This article is organized as the following: in Sec. II, we will describe our theoretical model and introduce a few physical quantities that are important in the investigation of phonon modes in QDs; in Sec. III, we will show our results and have discussions, and Sec. IV is a brief summary.

II. THEORETICAL APPROACH

The theoretical model we used to investigate phonon modes in QDs is a valence force field model (VFFM). In this

TABLE I. Calculated bulk phonon frequencies at high-symmetry points compared to experimental data (Ref. 35), all are in the unit of cm^{-1}.

	Γ(LO)	Γ(TO)	X(LO)	X(TO)	X(LA)	X(TA)	L(LO)	L(TO)	L(LA)	L(TA)
Exp.	239	217	203	216	160	53	203	216	140	44
Cal.	240	219	184	208	148	71	190	214	145	47

model, the change of the total energy due to the lattice vibration is considered as two parts, the change of the energy due to the short-range interactions and the change of the energy due to the long-range Coulomb interaction:

$$\Delta E = \Delta E_s + \Delta E_c, \qquad (2.1)$$

where the short-range part describes the covalent bonding, and the long-range part approximates the effective Coulomb interaction.

This treatment is similar to the model used in many calculations of phonon modes in semiconductor superlattices[26–31] and quantum wires,[32] and it is also similar to the approach employed in Ref. 25. We have used this model in a study of phonon modes in GaAs QDs.[33] For the short-range part, we employed a VFFM with only two parameters as the following:[34,35]

$$\Delta E_s = \sum_i \frac{1}{2} C_0 \left(\frac{\Delta d_i}{d_i} \right)^2 + \sum_j \frac{1}{2} C_1 (\Delta \theta_j)^2, \qquad (2.2)$$

where C_0 and C_1 are two parameters to describe the energy change due to the bond-length change and the bond angle change, respectively. The summation runs over all the bond lengths and bond angles. Because each of these two parameters has a simple and clear physical meaning, this model allows us to treat the interaction between atoms at the surface appropriately. It can be further used to treat the surface relaxation and reconstruction, as well as the surface and interface strain without much difficulties.

For the long-range Coulomb interaction, we have

$$E_c = \frac{1}{2} \sum_{i \neq j} \frac{e_i^* e_j^*}{|r_{ij}|}, \qquad (2.3)$$

where e^* is an effective charge introduced to describe the long-range Coulomb interaction,[36] and $|r_{ij}|$ is the distance between two ions i and j. The parameters C_0, C_1, and e^* we used for InAs are 41.0, 0.398, and 0.7052, and the calculated phonon frequencies together with corresponding experimental data[37] are listed in Table I. Considering the small number of parameters used in our model, our calculated results are reasonable with the correct trend. In this research, the fundamental effects of the quantum confinement are emphasized but not the exact phonon frequencies.

When considering the interaction between atoms, special attention is paid to atoms near the surfaces of the QDs. More specifically, for the short-range interaction, when an atom is located near the surface, interaction from its nearest-neighboring atom is considered only if that specific nearest atom is within the QD, and interaction from its second-neighboring atom is considered only if that specific second-

neighbor atom is in the QD, as well as the nearest-neighboring atom that makes the link between them. The second point is important, because it makes sense with the physics meanings of these two parameters, but it is easy to be neglected.

For the long-range Coulomb interaction, we also paid special attention to atoms near the surface. Because the total number of anions and cations in a QD might not be the same in our model, the entire QD might not be neutral in electric charge. Therefore, we performed our calculations based on two different approaches. First, we assume that atoms at the surfaces are the same as those in the bulk, i.e., they have the same charges, which is named as a natural charge approach. Second, we assume that the surface atoms take the charge that makes the QDs neutral that might be slightly different from those in the bulk. This one is named as the neutral charge approach. Our calculations show that these two approaches do not make a critical difference, and they give qualitatively similar results. Our results shown in this paper are from the natural charge approach.

One of the major difficulties in calculating phonons of QDs is its computational intensity. For example, when we calculate a InAs QD of size 8.5 nm, there are 11 855 atoms in it. Considering the three-dimensional vibration of each atom, the dynamic matrix is of the order of 35 565. This is an intimidating task even with the most advanced computer nowadays. We employed the projection operators of the irreducible representations of the group theory to reduce the computational intensity.[38–41] Then the above matrix of the size of 35 565 can be reduced to five matrices in five different representations of A_1, A_2, E, T_1, and T_2, with the sizes of 1592, 1368, 2960, 4335, and 4560, respectively. Therefore, the original problem is reduced to a problem that can be easily handled by most reasonable computers. This approach further allows us to investigate phonon modes with different symmetries in QDs in detail. These investigations lead to some interesting physics that we will discuss later.

Because the number of phonon modes in QDs is so huge, it is difficult to analyze them systematically. To gain some insights of these modes and to understand the vibration property of QDs in the real space in an intuitive way, we have introduced a few physical quantities to describe them. The first quantity introduced is the average vibration amplitude A_l^i of the lth shell in the ith phonon mode, which is defined as

$$A_l^i = \frac{1}{n} \sum_{k=1}^n |a_{lk}^i|, \qquad (2.4)$$

where a_{lk}^i is the vibration amplitude of the atom k in the lth shell in the ith phonon mode, and n is the total number of

TABLE II. The calculated highest frequencies of each of the five different representations of phonon modes in InAs QDs ranging from 8.57 to 84.98 Å. All the frequencies are in the unit of cm^{-1}.

Size(Å)	8.57	14.84	19.86	24.79	29.68	34.67	39.61	49.96	59.97	69.80	79.91	84.98
A_1	201.63	226.59	235.90	241.91	245.73	248.31	250.19	252.43	253.77	254.59	255.26	255.50
A_2		226.36	227.34	229.76	231.55	232.80	234.16	239.24	243.11	245.79	247.92	248.76
E	214.66	228.06	234.25	238.35	241.15	243.43	245.53	248.65	250.75	252.08	253.17	253.57
T_1	211.89	228.82	231.22	232.85	236.46	239.72	242.36	246.11	248.69	250.40	251.77	252.27
T_2	225.02	233.94	238.29	240.89	243.30	245.67	247.67	250.44	252.19	253.29	254.17	254.49

atoms in the lth shell. Some calculated results of the average vibration amplitudes in QDs will be shown in the next section.

The second physical quantity introduced is the radial ratio A_L^i/A^i, which is defined by

$$\frac{A_L^i}{A^i} = \frac{1}{N} \sum_{k=1}^{N} \frac{\left| a_k^i \cdot \dfrac{r_k}{|r_k|} \right|}{|a_k^i|}, \tag{2.5}$$

where a_k^i denotes the vibration amplitude of the kth atom in the ith mode, r_k is the position vector of the kth atom relative to the center of the QD, and N is the total number of atoms of the entire QD vibrating in that mode (please note that the N in 2.5 is different from the n in 2.4, which is the total number of atoms in one shell). This ratio describes to what extent a phonon mode, i.e., the ith mode, is radial-like. Two extreme cases of the radial ratios are 1 and 0, where ''1'' means that all atoms in the QDs in that specific mode vibrates in the radial directions, and ''0'' means that all atoms vibrates in planes perpendicular to the radial directions. In the next section, we will show some of our calculated results of radial ratios. Our results show that among the highest frequencies for a given QD, the A_1 mode has the largest radial ratio, as high as 0.987, and the A_2 has the lowest radial ratio, as low as 0.0454.

The third physical quantity introduced is an electric field ratio A_E^i/A^i. We know that in bulk semiconductors, long-wavelength LO modes would induce an oscillating macroscopic polarization that leads to an electric field. Similarly, in semiconductor QDs the opticlike modes may induce an electric dipole field in a site r in QDs. Let the e_l^* denotes the effective charge of the lth atom, then the dipole field induced on the site r_k due to the vibration of the ith mode is

$$E_k^i = - \sum_{l \neq k}^{N} \frac{e_l^* a_l^i}{|r_l - r_k|^3}, \tag{2.6}$$

where N is the total number of atoms in the QD, and a_l^i is the same as defined above. With this dipole field at site r_k, we can define the field ratio A_E^i/A^i in a way similar to the way we define the radial ratio A_L^i/A^i:

$$\frac{A_E^i}{A^i} = \frac{1}{N} \sum_{k=1}^{N} \frac{\left| a_k^i \cdot \dfrac{E_k^i}{|E_k^i|} \right|}{|a_k^i|}, \tag{2.7}$$

where all the quantities have been defined above. The field ratio is the average ratio of the displacement component of each atom along the direction of the local electric field at that site. Phonons with a large electric-field ratio will be more efficient in generating the macroscopic electric field. Therefore, it is more LO-like. On the other hand, phonons with smaller values of the field ratio are less LO-like. We have also calculated the field ratios for some phonon modes of QDs, and we will discuss them in the next section.

III. RESULTS AND DISCUSSIONS

We have calculated phonon modes in QDs of several semiconductor materials. Here we present our results for InAs QDs.

A. Size Effects on Frequencies of QDs with Different Symmetries

The size range we have calculated for InAs QDs is from 8.57 to 84.98 Å, which covers the most important and interesting range for the study of phonon modes in QDs. We do encounter a problem that when the size range of the QDs

TABLE III. The calculated lowest frequencies of each of the five different representations of phonon modes in InAs QDs ranging from 8.57 to 84.98 Å. All the frequencies are in the unit of cm^{-1}.

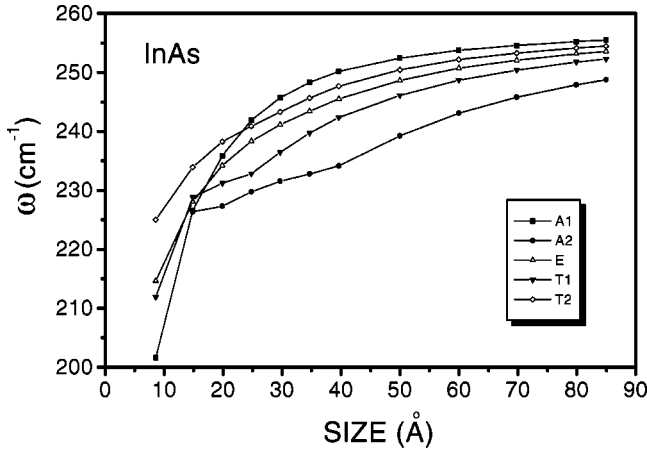| Size(Å)	8.57	14.84	19.86	24.74	29.68	34.67	39.61	49.96	59.97	69.80	79.91	84.98
A_1	48.70	43.36	47.68	38.60	33.49	32.00	28.65	24.16	21.70	19.87	17.98	17.49
A_2		19.50	23.78	25.85	19.75	18.16	16.58	15.51	13.70	12.31	11.48	11.03
E	16.30	21.65	20.28	17.86	15.87	14.52	13.38	11.75	10.58	9.67	8.70	8.29
T_1	10.12	4.65	10.37	9.22	7.13	5.69	5.37	4.34	3.54	2.82	2.34	1.84
T_2	29.45	26.27	30.97	25.18	22.62	21.20	19.03	16.52	14.67	13.46	12.19	11.74

FIG. 1. The highest frequencies in each of the five different symmetries for GaAs QDs with the size range from 8.57 to 84.98 Å. The symbols for all five symmetries are indicated. The crossover of the symmetries from A_1 to T_2 is at the size about 24.5 Å.
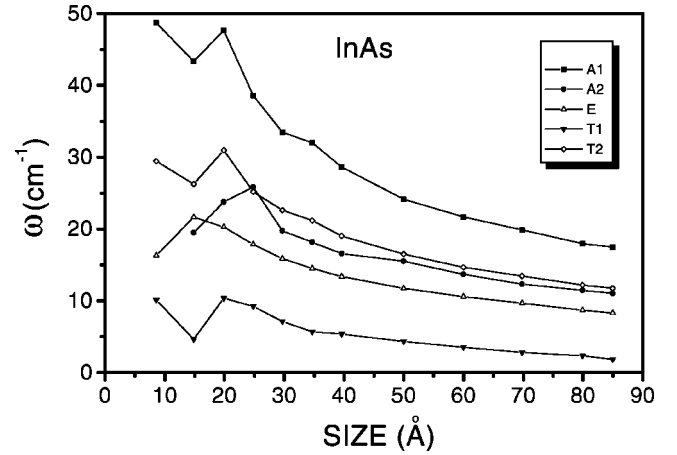

FIG. 2. The lowest frequencies in each of the five different symmetries for GaAs QDs with the size range from 8.57 to 84.98 Å. The symbols for all five symmetries are indicated.

increases, the highest frequency of QDs goes higher than the highest frequency of the bulk material, which conflicts the understanding that the bulk material can be considered as the limit of QD with infinitely large radius. More thoughts lead to the possibility that this is caused by the truncation at QDs surface and removal of the dangling bonds without changing the interaction parameters between atoms at the surface. Other than this, we have obtained many interesting results.

Next we will report our study of quantum confinements effect on phonon frequencies with different symmetries. The dependence of confinement effect of phonon frequencies on its symmetry causes a crossover of symmetries from A_1 to T_2 for the highest frequencies when the size of QDs decreases. We will also discuss the quantum confinement effect on the lowest frequencies when the size of the QDs changes.

As we discussed in the previous section, by employing the projection operators of the irreducible representation of the group theory, we are able to block diagonalize the entire lattice-dynamic matrix of the QD with a T_d symmetry into five small matrices that are in five different presentations (A_1, A_2, E, T_1, T_2). Then the five small matrices in each representation are diagonalized separately, and eigenvalues and eigenvectors are obtained in each representation, respectively.

In Tables II and III, we have listed the highest and lowest frequencies for each of the five representations of QDs with eleven different diameters. Because the zero frequency corresponds to a shift of the entire object, it is excluded from the lowest frequencies without losing any important physics.

These results are also shown in Figs. 1 and 2, where the highest and lowest frequencies of phonon modes are plotted against different sizes in each of the five symmetries. In general, we see that for all five different symmetries, the highest frequencies goes down and the lowest frequencies goes up as the size of the QDs decreases. This is due to the quantum confinement of phonon modes that is similar to the blueshift of the band gap for electronic states in semiconductor QDs. Another simple explanation comes from the uncertainty prin-

ciple. The smaller the sizes, the more uncertain the wave vectors. For bulk phonon modes, the highest frequency goes down and the lowest goes up when the wave vectors goes away from the center of the Brillouin zone. Therefore, a general trend is that the highest frequency of phonon modes in QDs goes down and the lowest one goes up as the size decreases. This quantum confinement effect of phonon modes in QDs has been discussed by several others.[25]

This quantum confinement effect can be further investigated in detail. First, we notice that the quantum confinement effect depends on the symmetry of the modes. For example, comparing the five curves in Fig. 1, we notice that the slope changes are different for the five symmetries, with A_1 obviously the biggest. This indicates that phonon modes with different symmetries in QDs have different quantum confinement effect, with A_1 the strongest. More detailed study tells us that T_1 states have the weakest confinement effect. Because of the dependence of quantum confinement effect on symmetry, there is a crossover of symmetry of the highest frequency in QDs from A_1 to T_2 at the size of about 23.5 Å. Therefore, for QDs with a size larger than 23.5 Å, the highest frequency is a A_1 mode; and for QDs with a size smaller than 23.5 Å, the highest frequency is a T_2 mode. This type of crossover can be further explained as the following:

Since the phonons of QDs are derived from bulk phonons, it always helps to understand the QDs phonons starting from the bulk phonons. In bulk InAs, there is a splitting of the LO and TO at the Γ point due to the long-range Coulomb interaction. Without Coulomb interaction, the LO and TO modes would be a triple degenerate mode at the Γ point. For $\vec{k}$ in the [1,0,0] and its equivalent directions (six in total and are indicated as $\langle 1,0,0 \rangle$), the phonon spectra splits into a double degenerate $\Delta_3 + \Delta_4$ branch (TO) and a nondegenerate Δ_1 branch (LO); of these two, the Δ_1 branch has a larger dispersion than the $\Delta_3 + \Delta_4$ branch, i.e., the LO frequencies decrease faster than the TO frequencies when the $\vec{k}$ goes away from the Γ point. This is true with or without the Coulomb interaction. For $\vec{k}$ in the [1,1,1] and its equivalent directions (four in total, and are indicated as $\langle 1,1,1 \rangle$), the

bulk spectra splits into a double degenerate Λ_3 (TO) and a nondegenerate Λ_1 (LO), of which the LO branch has a larger dispersion than the TO branch, with or without the Coulomb interaction.

For QDs with limited size, their frequencies are composed of many bulk states $|n,\vec{k}\rangle$ with $\vec{k} \neq 0$, which frequencies are lower than the frequencies at the Γ point. Particularly, for six $\langle 1,0,0 \rangle$ directions, the linear combination of the LO states $|\Delta_1,\vec{k}\rangle$ gives one A_1 state, one double degenerate E state, and one triple degenerate T_2 state. We can write this relation as

$$6|\Delta_1,\vec{k}_\Delta\rangle \Rightarrow A_1 + E + T_2. \qquad (3.1)$$

Similarly, for $\langle 1,0,0 \rangle$ TO modes we have

$$6|\Delta_3 + \Delta_4,\vec{k}_\Delta\rangle \Rightarrow 2T_1 + 2T_2. \qquad (3.2)$$

For $\langle 1,1,1 \rangle$ LO modes, we have

$$4|\Lambda_1,\vec{k}_\Lambda\rangle \Rightarrow A_1 + T_2, \qquad (3.3)$$

and for $\langle 1,1,1 \rangle$ TO modes, we have

$$4|\Lambda_3,\vec{k}_\Lambda\rangle \Rightarrow E + T_1 + T_2. \qquad (3.4)$$

These equations play an important role in our later argument.

As the size of the QDs decreases, the highest frequencies of all five different representations will go down, however, they are going down at different rates. Since the bulk LO branch has a larger dispersion than the TO branch, the LO related modes would have a greater size effect than the TO related modes.

From above equations (3.1–3.4) we see that the A_1 modes of QDs are only affected by the bulk LO modes, and the T_1 modes of QDs are only affected by the bulk TO modes, while the T_2 modes are affected by both the bulk LO and TO modes. Therefore, the A_1 modes would have the strongest size effect, T_1 modes the weakest, with the T_2 modes in between. So, even though in the bulk GaAs the A_1 modes have the highest frequency, because the highest A_1 frequency goes down at a rate faster than the highest T_2 frequency as the size of QDs decreases, at a certain size, the highest A_1 frequency might be even lower than the highest T_2 frequency. This would cause the crossover of symmetries for the highest frequency from A_1 to T_2. For InAs QDs, this happens at the size of about 23.5 Å. This argument is not based on any specific theoretical model or any specific material, so it is model independent and it applies to all materials with the Zinc-blende structure. Because the crossover is closely related to the dispersion of the bulk LO and TO spectra, the specific size of the possible crossover depends on the ratio of these two dispersions. In general, when the ratio is big, the crossover will happen for QDs at a large size, and *vice versa*.

For the lowest frequencies in Fig. 2, the lowest frequencies for all five representations go up as the size of QDs decreases, with some fluctuations when the size is less than 20 Å. This going up is due to the quantum confinement, and we think that the fluctuations are due to the calculation ac-

curacy when the frequency is low, and the VFFM may not apply well when the size of QDs is so small. Again we notice that, for these lowest frequencies, the states with different symmetries have different quantum confinement effect, with A_1 the strongest and T_1 the weakest. For the lowest frequencies, there is no crossover. This can be understood in detail from the property of bulk phonons.

For bulk phonon modes, there is a triple degenerate zero frequency at Γ point and it splits into a double degenerate $\Delta_3 + \Delta_4$ branch (TA) and a nondegenerate Δ_1 branch (LA) for $\vec{k}$ in the $\langle 1,0,0 \rangle$ directions and splits into a double degenerate Λ_3 (TA) and a nondegenerate Λ_1 (LA) for $\vec{k}$ in the $\langle 1,1,1 \rangle$ directions. Then the same argument as the highest frequencies can apply. Because the bulk LA modes have bigger dispersion (speed of sound) than the TA mode, which is true for most materials, the A_1 modes go up the fastest and the T_1 mode the lowest. This is obvious in the figure. However, the lowest state of the bulk material is a triple degenerate T_2 state at Gamma point with a zero frequency, which exists for QDs of all sizes. This zero frequency was excluded from our discussion because it corresponds to a shift of the whole object. Since T_1 always goes up the slowest, the lowest frequency stay as a T_1 state when the size of the QDs decreases.

In general, for both the highest and lowest frequencies, as long as the longitudinal modes have a larger dispersion than the transverse modes, the rule of the extent of confinement $A_1 > T_2 > T_1$ in quantum confinement applies. Our calculated results of phonon modes in InAs QDs prove that.

The size effect of phonon frequencies of QDs have been studied by other microscopic models[25,42] and the continuum dielectric model.[21–23] The general trend that the high frequencies decrease as the size of QDs decreases was discussed by other models. But the size range of the QDs covered by other microscopic models[25] is limited to about 2000 atoms due to the computational intensity as we have discussed before, and the different quantum confinement effects for modes with different symmetries could not be revealed without applying the group theory. The dielectric models have the advantage of giving analytical results that can be conveniently used in the study of electron-phonon interaction and other interactions with phonons, and they can also be used to study the macroscopic interface modes of QDs.[15] The continuum dielectric model coupling (CDMC), the mechanical vibrational amplitudes and the electrostatic potential (Ref. 21) has made major improvements over classical dielectric models in the study of phonon modes in QDs, and have discussed several features that we have discussed here. For example, CDMC has predicated that the frequencies of the coupled mode with $l = 0$ reduces as the radius of GaAs sphere decreases, which is similar to what was predicted by our VFFM. In addition to this quantum effect, the coupled modes of $l = 0$ are radial modes and have the most important contribution to one-phonon Raman scattering. Their frequencies approach the frequency of LO phonon at the center of the Brillouin zone of bulk GaAs when the size of the GaAs QDs is large. Furthermore, the CDMC has predicted that the uncoupled modes to be torsional modes of pure transverse

character, and their frequencies approach to the TO phonon at the center of the Brillouin zone of bulk GaAs when the size tends to be large. To better compare our results with these results of CDMC, we have generalized our program to investigate phonon modes in GaAs QDs embedded in AlAs shells of certain thickness, which we call GaAs/AlAs shell-QDs. The results are identified and compared with the CDMC results. We have also designed a k-space projection scheme[38-41] that projects the modes of QDs into the bulk modes in the Brillouin zone. Our primitive results show that the phonon modes of GaAs/AlAs shell-QDs of VFFM with A_1 symmetry have strong projection into bulk GaAs LO modes, while modes with T_1 symmetry have strong projection into bulk TO modes. It is expected that that the phonon modes of shell-QDs of VFFM with A_1 symmetry should have strong projection into the $l=0$ coupled mode of CDMC, while VFFM modes with T_1 symmetry should have stronger projection into the uncoupled modes of CDMC. We have also obtained some interesting results, such as the microscopic interface modes in GaAs/AlAs shell-QDs, that could not be revealed by the macroscopic dielectric model due to its fundamental limitation of neglecting the bonding and anisotropy of the crystal structure of QDs. The detail of the identification and comparison is beyond the scope of this paper and will be published elsewhere.[43]

B. Vibration Amplitudes and Vibration Energies of Phonon Modes in QDs

We have also calculated the vibration amplitudes and vibration energies of all atoms for all phonon modes. In order to understand these atomic vibrations in real space in an intuitive way, we have plotted the average amplitudes as functions of shell radius for the highest frequency of each of the five symmetries. The physical meaning of the average amplitude is defined in Sec. II. The results are shown in Figs. 3–7 in the order of A_1, A_2, E, T_1, and T_2. For each symmetry, we studied QDs with three different sizes: 30 Å (a), 60 Å (b), and 85 Å (c). The sizes listed here are in diameters, but the sizes shown in Figs. 3–7 are radius that go from the center of the QDs to the surface.

We first look at Fig. 3 in detail, that is for the A_1 mode. One thing we notice is that even though these three figures (a)–(c) have different details, they all have a similar shape in general. More specifically, the average amplitudes for all three different sizes are zeros at the center of the QDs and very small at the surfaces, with the maximum of the average amplitudes in the middle range of the radius. The vibration amplitude is equal to zero at the center of the QDs for A_1 state, because there is only one atom at the center of the QDs, and its three-dimensional vibration is a T_2 state. Since there is no A_1 state at the center of the QDs, its vibration amplitude is of course zero. The second thing we notice is the zigzag-shaped average vibration amplitudes, and there are obviously two envelope functions for the entire range. This can be easily explained by the momentum conservation and the different masses of In atoms and As atoms ($m_{In}=114$ amu, and $m_{As}=75$ amu). In optical modes, the momentum of In atoms and As atoms have the same norm, but
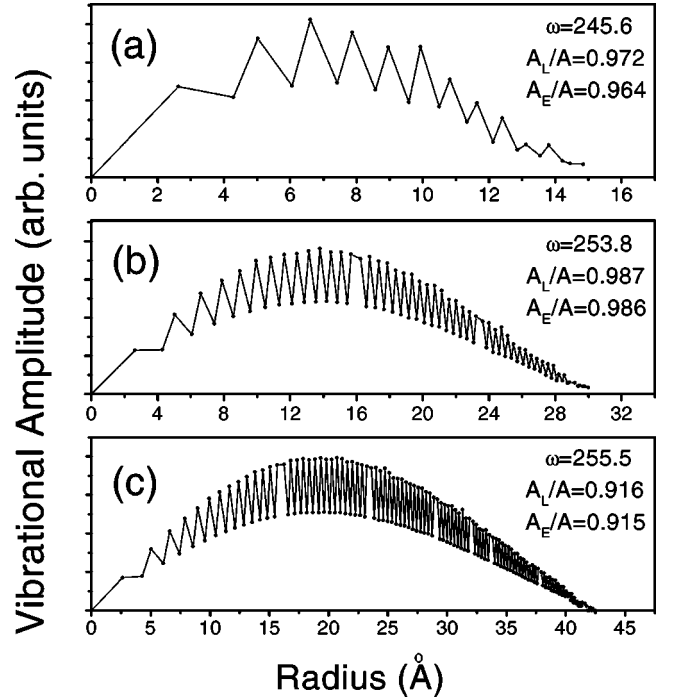

FIG. 3. Average vibration amplitudes as a function of shell radius for the A_1 mode with the highest frequency in QDs of size 30Å (a), 60Å (b), and 85Å (c).

are in opposite directions, thus the center of mass of the two atoms keeps static. In a phonon mode, the vibration amplitude of an atom is proportional to its momentum. If we multiply the average amplitude of the In shells with the mass of the In atom and that of the As shells with the mass of the As atom, we will get quite a smooth curve for the entire size range. This feature makes sense only if all atoms with the same distance to the center are the same type of atoms, either In or As, but not mixed. Checking with the data files we found that this is true for the entire size range of our investigations up to about 85 Å. We have also noticed that there are a few broken-ups of the general rule of ups and downs next to each other. For example, we notice that there are two ups next to each other at the radius of about 16 and 23.5 Å in Fig. 3(b). The only possibility is that at these two sizes there are two shells next to each other with the same type of atoms. Checking with the data files also proves it.

In each of these figures, three physical quantities are given: the frequency of the mode, which is the highest frequency of this symmetry in QDs with this size; the average radius ratio, and the average electric field ratio. The physical meanings of the latter two are defined in Sec. II. The numbers listed in Fig. 3(a)–3(c) are for the A_1 modes with the highest frequencies, of them the average amplitudes are plotted. We see that both the average radius ratio and the average field ratios are close to one for all three sizes, that indicates that these A_1 modes are quite radial like, and they are also LO-like.

The next few figures, Figs. 4–7, are parallel to Fig. 3, but they correspond to four other different symmetries. Looking at Fig. 4, which is for A_2 modes, we notice again that the centers of the QDs have a zero vibration amplitude, and the
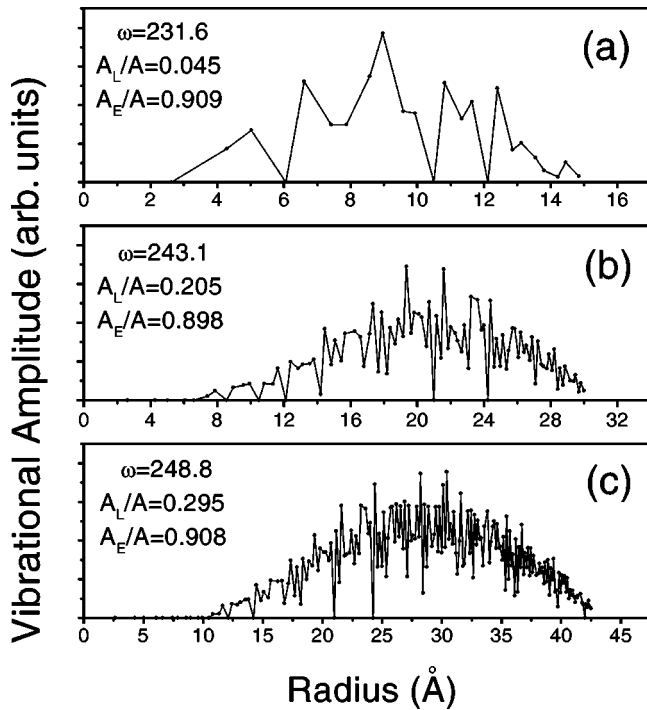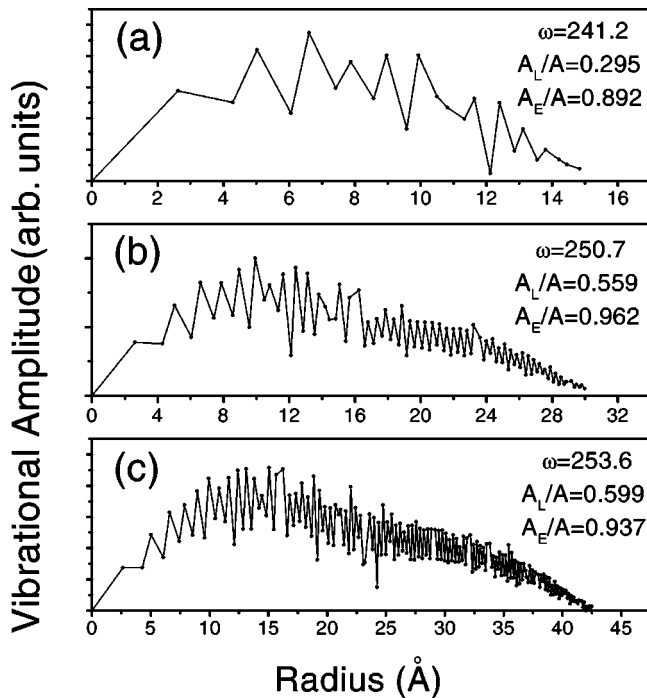
FIG. 4. Average vibration amplitudes as a function of shell radius for the A_2 mode with the highest frequency in QDs of size 30Å (a), 60Å (b), and 85Å (c).
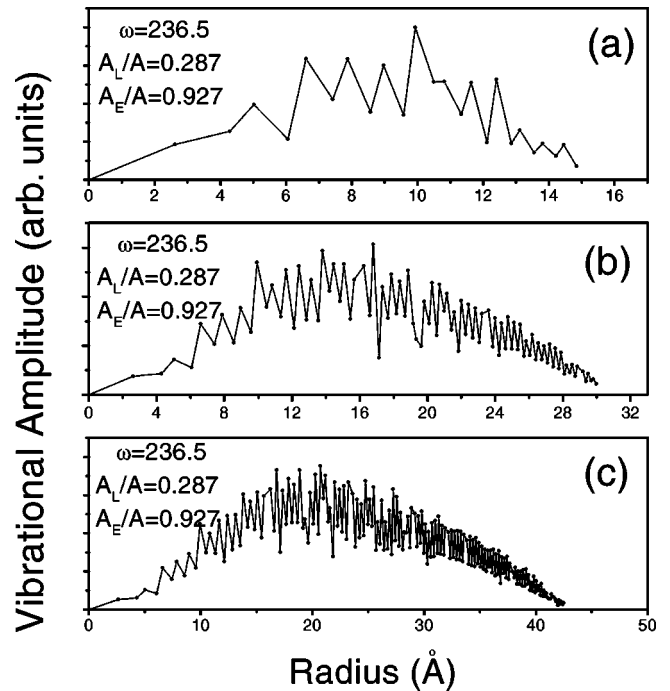

FIG. 6. Average vibration amplitudes as a function of shell radius for the T_1 mode with the highest frequency in QDs of size 30Å (a), 60Å (b), and 85Å (c).

surface atoms have very small average amplitudes. Other than that, we also notice that there are several zero vibration amplitudes, at the radius of 2.6, 6.1, 10.5, and 12.1 Å, etc. Checking the data files we found that because of the symme-

try property of atoms at those shells, there is no A_2 mode at these radius. Therefore, the average vibration amplitude of A_2 modes must be zero. Another big difference between Fig. 3 and Fig. 4 is the values of radial ratios, which in Fig. 4 are
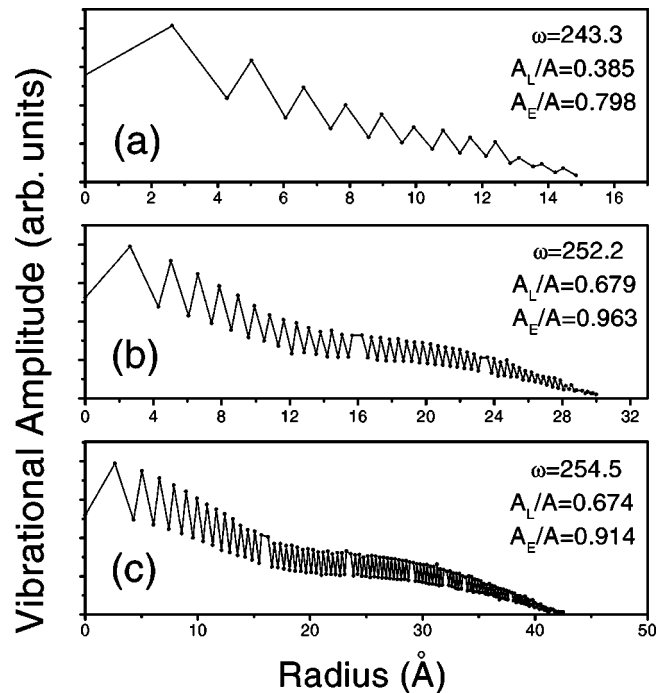

FIG. 5. Average vibration amplitudes as a function of shell radius for the E mode with the highest frequency in QDs of size 30Å (a), 60Å (b), and 85Å (c).

FIG. 7. Average vibration amplitudes as a function of shell radius for the T_2 mode with the highest frequency in QDs of size 30Å (a), 60Å (b), and 85Å (c).

much smaller than in Fig. 3. This indicates that the A_2 modes have more vibration components in planes perpendicular to the radius.

Figs. 5, 6, and 7 are for E, T_1, and T_2 modes, respectively. There is one special feature we want to point out in Fig. 7, which is for T_2 modes. Unlike all other symmetries, the highest-vibration amplitude in T_2 modes is located at the center of the QDs. That is because there is only one atom at the center of the QD, and its three-dimensional vibration is a T_2 mode. We also notice that the E, T_1, and T_2 modes have a radial ratio between A_1 and A_2, and all of these modes have high electric-field ratios.

To investigate the distribution of vibration energy in a phonon mode, we have introduced another physical quantity $\widetilde{A}_l^i$, which is the mean-square root of the vibration amplitude of the lth shell in the ith phonon mode:

$$\widetilde{A}_l^i = \left[\frac{1}{n} \sum_{k=1}^{n} (a_{lk}^i)^2 \right]^{1/2}. \tag{3.5}$$

This quantity is related to the average vibration energy E_l^i by

$$E_l^i \propto m_l \times \widetilde{A}_l^{i\,2}. \tag{3.6}$$

We performed calculations of this quantity for the highest frequencies of each of the five symmetries of QDs with size of 30, 60, and 85 Å, and plotted them as we did in Figs. 3–7. The results show that the curves for $\widetilde{A}_l^i$ and the average vibration amplitude A_l^i have quite similar structures, both the shape and the zigzag-shaped details. When we plot them together in the same figure, we can hardly tell their difference. Hence, these results are not shown here due to their similarity to Figs. 3–7.

In general, above shown are some of the microscopic details of the phonon modes in QDs that we have learned from our microscopic model. Based on these microscopic details, many physical properties of the semiconductor QDs can be further investigated.

IV. SUMMARY

In summary, we have applied a simple valence force field model to investigate phonon modes in InAs QDs. The irreducible representations of the group theory are employed to reduce the computational intensity, which further leads to some interesting physics that otherwise cannot be revealed. We have found that the size effect of quantum confinement depends on symmetries of the modes, with A_1 the strongest, and T_1 the weakest. This causes a crossover of symmetries of the highest frequencies from A_1 to T_2 in InAs QDs at the size of about 23.5 Å. Not only are we able to obtain all the vibration frequencies of QDs, but also we have calculated all the vibration amplitudes of all atoms directly from the dynamic matrices. The microscopic details of the vibration amplitudes and vibration strengths are investigated. With these microscopic description of phonon modes in QDs, we can further calculate many other physics quantities of QDs, such as the electron-phonon interaction, phonon-assisted carrier relaxation, Raman scattering, and light emission, etc., and compare our results with the some related experimental measurement. These are our future goals.

[1] A.D. Yoffe, Adv. Phys. **42**, 173 (1993).

[2] S. Hayashi, H. Sanda, M. Agata, and K. Yamamoto, Phys. Rev. B **40**, 5544 (1989).

[3] M.J. Steer, D.J. Mowbray, W.R. Tribe, M.S. Skolnick, M.D. Sturge, M. Hopkinson, A.G. Cullis, C.R. Whitehouse, and R. Murray, Phys. Rev. B **54**, 17 738 (1996).

[4] A. Roy and A.K. Sood, Phys. Rev. B **53**, 12 127 (1996).

[5] M. Fujii, S. Hayashi, and K. Yamamoto, Appl. Phys. Lett. **57**, 2692 (1990).

[6] A. Tanaka, S. Onari, and T. Arai, Phys. Rev. B **45**, 6587 (1992).

[7] S. Hayashi and R. Ruppin, J. Phys. C **18**, 2583 (1985).

[8] S. Hayashi and H. Kanamori, Phys. Rev. B **26**, 7079 (1982).

[9] A. Tanaka, S. Onari, and T. Arai, Phys. Rev. B **47**, 1237 (1993).

[10] M.C. Klein, F. Hache, D. Richard, and C. Flytzanis, Phys. Rev. B **42**, 11 123 (1990).

[11] A.M. Depaula, L.C. Barbosa, C. Cruz, O.L. Alves, J.A. Sanjurjo, and C.L. Cesar, Appl. Phys. Lett. **69**, 357 (1996).

[12] C.M. Dai and D.S. Chuu, Solid State Commun. **81**, 387 (1992).

[13] G. Tamulaitis, P.A.M. Rodrigues, and P.Y. Yu, Solid State Commun. **95**, 227 (1995).

[14] B. Champagnon, B. Andrianasolo, and E. Duval, Mater. Sci. Eng., B **9**, 417 (1991).

[15] P.A. Knipp and T.L. Reinecke, Phys. Rev. B **48**, 18 037 (1993).

[16] Y.N. Hwang, S.H. Shin, H.L. Park, S.H. Park, U. Kim, H.S. Jeong, E.J. Shin, and D. Kim, Phys. Rev. B **54**, 15 120 (1996).

[17] H. Frohlich, *Theory of Dielectrics, Dielectric Constant, and Dielectric Loss* (Oxford University Press, Oxford, 1949).

[18] R. Fuchs and K.L. Kliewer, Phys. Rev. **140**, A2076 (1965).

[19] R. Ruppin and R. Englman, Rep. Prog. Phys. **33**, 149 (1970).

[20] C. Trallero-Giner, F. Garcia-Moliner, V.R. Velasco, and M. Cardona, Phys. Rev. B **45**, 11 944 (1992).

[21] E. Roca, C. Trallero-Giner, and M. Cardona, Phys. Rev. B **49**, 13 704 (1994).

[22] M.P. Chamberlain, C. Trallero-Giner, and M. Cardona, Phys. Rev. B **51**, 1680 (1995).

[23] C. Trallero-Giner, A. Debernardi, M. Cardona, E. Menendez-Proupin, and A.I. Ekimov, Phys. Rev. B **57**, 4664 (1998).

[24] W.S. Li and C.Y. Chen, Physica B **229**, 375 (1997).

[25] H. Fu, V. Ozolins, and A. Zunger, Phys. Rev. B **59**, 2881 (1999).

[26] S.F. Ren, H.Y. Chu, and Y.C. Chang, Phys. Rev. Lett. **59**, 1841 (1987).

[27] S.F. Ren, H.Y. Chu, and Y.C. Chang, Phys. Rev. B **37**, 8899 (1988).

[28] H.Y. Chu, S.F. Ren, and Y.C. Chang, Phys. Rev. B **37**, 10 746 (1988).

[29] S.F. Ren, H.Y. Chu, and Y.C. Chang, Phys. Rev. B **40**, 3060 (1989).

[30] S.F. Ren and Z.Z. Xu, Solid State Commun. **104**, 435 (1997).

[31] Z.Z. Xu, H. Dowd, S.F. Ren, and Z.Q. Gu, J. Phys.: Condens. Matter **9**, 1539 (1997).

[32] Optical phonons in GaAs/AlAs quantum wires, S.F. Ren and Y.C. Chang, Phys. Rev. B **43**, 11 857 (1991).

[33] S.F. Ren, Z.Q. Gu, and D.Y. Lu. Solid State Commun. **113**, 273 (2000).

[34] W.A. Harrison, *Electronic Structure and the Properties of Solids* (Freeman, San Francisico, 1980).

[35] P. Yu and M. Cardona, *Fundamentals of Semiconductors, Physics and Materials Properties* (Springer, Berlin, 1996).

[36] K. Kunc, M. Naalkanski, and M. Nusimovici, Phys. Status Solidi B **72**, 229 (1975); K. Kunc, Ann. Phys. (Paris) **8**, 319 (1973).

[37] *Semiconductors-Basic Data*, edited by Otfried Madelung (Springer, Berlin, 1996).

[38] S.Y. Ren, Phys. Rev. B **55**, 4665 (1997).

[39] S.Y. Ren, Solid State Commun. **102**, 479 (1997).

[40] S.Y. Ren, Jpn. J. Appl. Phys., Part 1 **36**, 3941 (1997).

[41] S.Y. Ren and S.F. Ren, J. Phys. Chem. Solids **59**, 1327 (1998).

[42] J. Zi, H. Buscher, C. Falter, W. Ludwig, K. Zhang, and X. Xie, Appl. Phys. Lett. **69**, 200 (1996).

[43] G. Qin and S. F. Ren (unpublished).